Dynamic phase transitions in simple driven kinetic networks

Suriyanarayanan Vaikuntanathan,[1] Todd R. Gingrich,[2] and Phillip L. Geissler[1,2,3]
[1]*Material Sciences Division, Lawrence Berkeley National Laboratory, Berkeley, California 94720, USA*
[2]*Department of Chemistry, University of California, Berkeley, Berkeley, California 94720, USA*
[3]*Chemical Sciences Division, Lawrence Berkeley National Laboratory, Berkeley, California 94720, USA*
(Received 12 July 2013; revised manuscript received 14 May 2014; published 5 June 2014)

We analyze the probability distribution for entropy production rates of trajectories evolving on a class of out-of-equilibrium kinetic networks. These networks can serve as simple models for driven dynamical systems, where energy fluxes typically result in nonequilibrium dynamics. By analyzing the fluctuations in the entropy production, we demonstrate the emergence, in a large system size limit, of a dynamic phase transition between two distinct dynamical regimes.

DOI: 10.1103/PhysRevE.89.062108 PACS number(s): 05.70.Ln, 05.40.−a, 05.70.Fh, 82.40.Bj

The study of fluctuation phenomena is one of the central endeavors of nonequilibrium statistical mechanics. The analysis of fluctuations in nonequilibrium processes has, for example, led to the discovery of the fluctuation theorems, which have helped elucidate how macroscopic notions of irreversibility emerge from microscopic laws [1–3]. More recently, theoretical and numerical analyses of the statistics of rare fluctuations in driven lattice gas models [4,5], exclusion processes [6], zero-range processes [7], one-dimensional models of transport [8], and models of glass formers [9,10] have revealed the presence of coexisting ensembles of trajectories and so-called dynamic phase transitions between them [4,5,8,11]. In this paper we analyze the statistics of rare fluctuations in entropy production rates for certain model nonequilibrium, or driven, kinetic networks (see Fig. 1). While this Markovian system, with effectively one-particle dynamics, lacks much of the complexity of previously studied driven systems [4–8], we show, numerically and analytically, the presence of two dynamical phases, each with a characteristic entropy production rate. This demonstration shows that singularities in trajectory space can in fact arise even in very simple driven kinetic networks with a single degree of freedom. Driven kinetic networks of this general flavor are used to model a variety of physical, chemical, and biological systems including molecular motor dynamics [12,13]; cellular feedback, control, and regulation [14]; and kinetic proofreading mechanisms [15,16]. Physically, the dynamic phase transition serves to enhance the probability of observing large fluctuations in the dynamical behavior of these hopping processes.

We study dynamical fluctuations of a system evolving on cyclical or periodic driven kinetic networks with some heterogeneity in the transition rates. We consider two types of cyclic networks, which we hereafter refer to as the ring network and the triangle network. The ring network connects N states in a circle with transition rates x in the clockwise direction and 1 in the reverse direction. The network has translational symmetry, but we also construct a variation of the ring network with that symmetry broken by a link we call the heterogeneous link, or h link. As shown in Fig. 1(a), this link connects states 1 and N with rate h in each direction. The triangle networks are similar in structure but consist of triangular motifs as depicted in Fig. 1(b). Each triangular motif has one asymmetric link with rates $x \neq y$ resulting in cycling currents on average. Triangular subunits offer both driven and undriven paths between sites on their horizontal edge.[1] The important motivation for considering this decoration is to establish a generality that includes cases in which detailed balance is violated locally as well as globally.

To demonstrate the presence of multiple dynamical phases, we focus on fluctuations in the entropy production rate σ in the large-N limit. This rate is of particular physical interest since it is a measure of the power provided by external sources to drive the system through the network in a manner that violates detailed balance. A trajectory on our network corresponds to a series of Poissonian transitions, or hops, along links with forward and reverse rate constants k_f and k_r, respectively. The total entropy, in units of k_B, produced as the system evolves along a particular trajectory is given by [18]

$$\omega = \sum_{\text{hops}} \ln \frac{k_f}{k_r}. \tag{1}$$

We first describe numerically sampled steady-state trajectories, of length τ, and the resulting probability distribution $P(\sigma)$ of the entropy production rate $\sigma \equiv \omega/\tau$. In Fig. 2 we plot $\ln P(\sigma)$ for both the translationally symmetric triangle network and the triangle network with the heterogeneous link, as measured by kinetic Monte Carlo simulations [19]. For entropy production rates above a critical value $\sigma_h^* \approx 2.3$, the probability densities $P(\sigma)$ of the translationally symmetric and heterogeneous networks are almost identical. In fact, the most probable entropy production rate is largely unaffected by the broken symmetry. However, for entropy production rates lower than σ_h^*, $P(\sigma)$ of the heterogeneous network differs from its translationally symmetric counterpart by a "fat tail," which indicates the presence of a second distinct dynamical phase, whose entropy production rate is centered around $\sigma_l^* \approx 0.2$.

To clarify the nature of these dynamical phases, we harvested a long trajectory on the heterogeneous network with a value of σ between σ_l^* and σ_h^*. This trajectory, shown as an inset in Fig. 2, illustrates a switching between two types of behaviors. Initially the trajectory is localized and generates entropy at a rate of roughly σ_l^* as it cycles around triangular motifs near the h link. Eventually the trajectory escapes

[1]Such motifs were introduced, for example, in some of the earliest models of kinetic proofreading [15,17].

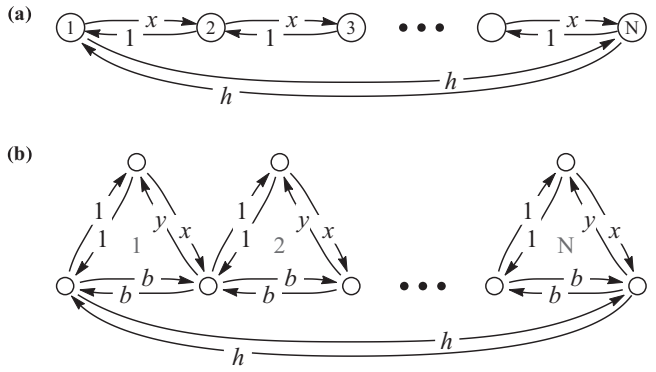

FIG. 1. Diagrams of simple driven kinetic networks studied here. Arrows connecting a pair of vertices indicate Poisson-distributed transitions from one state to the other, labeled by the corresponding rate constants.

through the h link and rapidly cycles around the entire network while generating entropy at a rate of approximately σ_h^*. For very small values of h, the behavior is explained simply: A bottleneck that hinders repeated cycling through the network should clearly produce some degree of transient stalling. In Fig. 4, however, we illustrate that the fat tail in the entropy production distribution persists even when h is not small relative to the other rates. Furthermore, the simple bottleneck explanation does not transparently reveal the emergence of a true phase transition in trajectory space.

To understand the dynamical fluctuations more generally it is productive to view the h link as an impurity among otherwise translationally symmetric units. This impurity breaks symmetry and enables trajectories to be split into two distinct classes. One class looks like the ordinary random walkers on the translationally symmetric network with the typical

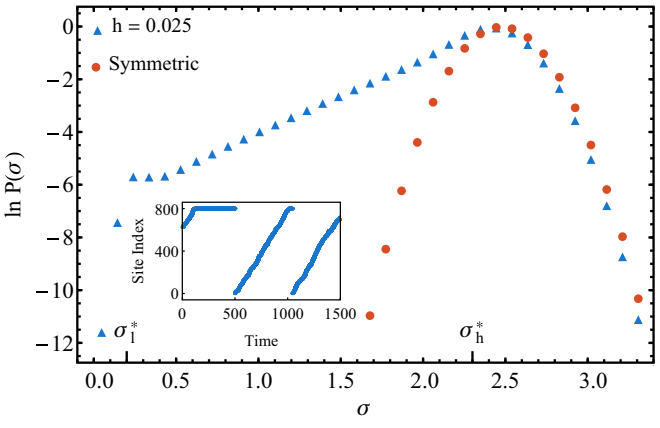

FIG. 2. (Color online) Entropy production distribution for the translationally symmetric triangle networks (red circles) and triangle networks with the heterogeneous link [see Fig. 1(b)] (blue triangles). For each network, 10^7 independent trajectories of length $\tau = 250$ were generated with $x = 20$, $y = 1$, $b = 0.1$, $h = 0.025$, and $N = 400$. The inset shows a trajectory illustrating the two dynamical regimes. Sites are numbered clockwise in a zig-zag fashion with the h link connecting sites 1 and 800.

trajectory not stalling around the heterogeneity, but the second class localizes around the impurity even when $h > x$.

In order to gain analytical insight into the nature of the dynamic phase transition, we consider the scaled cumulant generating function [20,21] of the entropy production,

$$\psi_\omega(\lambda) = \lim_{\tau\to\infty} \frac{1}{\tau} \ln\langle e^{-\lambda\omega}\rangle, \tag{2}$$

where the expectation value is taken over trajectories initialized in the steady-state distribution. In the limit of large τ, the probability of observing a particular value of entropy production obeys a large deviation principle [21]

$$P(\sigma) \approx e^{-\tau I(\sigma)}, \tag{3}$$

where $I(\sigma)$ is the large deviation rate function. For finite τ, $P(\sigma)$ can in principle be determined by sampling trajectories as described above. Deviations from $\sigma = \langle\sigma\rangle$ become extremely rare, however, as τ grows, so the limiting form of $I(\sigma)$ is impractical to determine by straightforward simulation. Alternatively, the convex envelope of $I(\sigma)$ can be computed as the Legendre-Frenchel (LF) transform of $\psi_\omega(\lambda)$ [20,21]. Following the general framework laid out by Lebowitz and Spohn [21], we calculate $\psi_\omega(\lambda)$ as the maximum eigenvalue of a matrix operator $\mathbb{W}_\omega(\lambda)$, which is simply related to $\mathbb{W}$, the transition matrix for the kinetic network [21]. Specifically, the matrix elements of the so-called tilted operator are given by

$$\mathbb{W}_\omega(\lambda)_{ij} = (1-\delta_{ij})\mathbb{W}_{ij}^{1-\lambda}\mathbb{W}_{ji}^{\lambda} + \delta_{ij}\mathbb{W}_{ij}. \tag{4}$$

By solving for the eigenspectrum of $\mathbb{W}_\omega(\lambda)$ we obtain $\psi_\omega(\lambda)$ and therefore the envelope of $I(\sigma)$ via the LF transform. Furthermore, the form of the maximal eigenvector reflects the character of the dominant trajectories, which will not be addressed in the present work.

Consistent with the two-phase behavior suggested by our simulation results, numerical eigenvalue calculations for the heterogeneous networks indicate that $\psi_\omega(\lambda)$ develops a cusp at some critical value λ^* in the large-N limit. A second cusp at $1-\lambda^*$ is necessitated by the symmetry of $\psi_\omega(\lambda)$ about $\lambda = 1/2$ [21]. The emergence of the cusps as N is increased is demonstrated by plots of $\psi_\omega(\lambda)$ as a function of λ for the triangle network at multiple values of N in Fig. 3(a). Plots of $\langle\sigma\rangle_\lambda \equiv -\partial\psi_\omega(\lambda)/\partial\lambda$ in Fig. 3(b) highlight the sharp decrease in the first derivative of the cumulant generating function near $\lambda = \lambda^*$, which trends towards a discontinuous jump as N increases. The discontinuous change in $\langle\sigma\rangle_\lambda$ signals a dynamic phase transition, wherein trajectories switch between the characteristic entropy production rates σ_h^* and σ_l^* for the two coexisting dynamical phases, in response to a small change in λ. We also evaluated $\psi_\omega(\lambda)$ and $\langle\sigma\rangle_\lambda$ at multiple values of h with fixed N. These results, collected in Figs. 3(c) and 3(d), show that the general features described above are present for all the values of h considered and that h serves to tune the critical value of λ. While it is not straightforward to physically bias the λ field (it couples to a time-nonlocal order parameter), the singularity in $\psi_\omega(\lambda)$ provides significant information about the large fluctuations in the natural dynamics.

Indeed, the cusp in $\psi_\omega(\lambda)$ when $N \to \infty$ implies that the region of the large deviation function between the entropy rates σ_h^* and σ_l^* is connected by a Maxwell construction (or a tie line) with a slope λ^*. The LF transform of $\psi_\omega(\lambda)$ only provides the

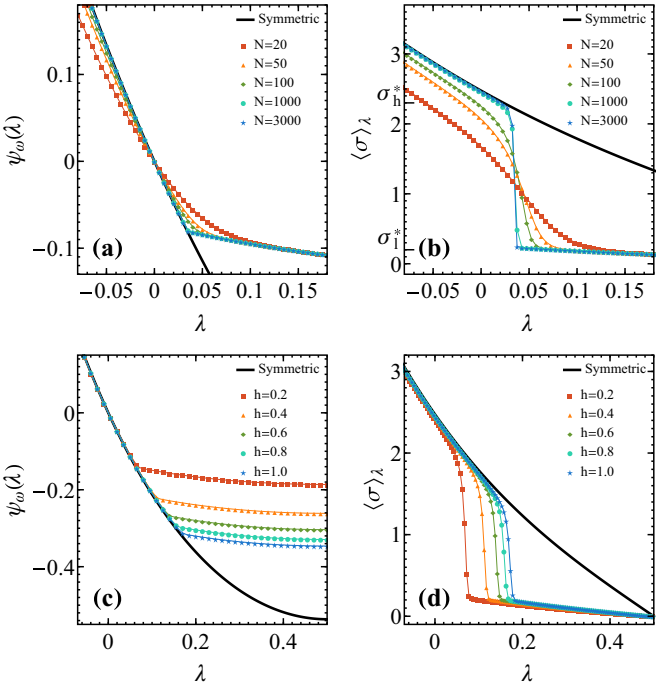

FIG. 3. (Color online) Scaled cumulant generating functions and average entropy production rates for the triangle networks, depicted in Fig. 1(b). All results are shown for rates $x = 20$, $y = 1$, and $b = 0.1$. Black solid curves show the exact behavior of the symmetric variant for comparison. Plots (a) and (b) show results for a variety of network sizes with $h = 0.1$ for the symmetry-breaking link, suggesting a singularity in the large-N limit. Plots (c) and (d) show results for $N = 200$ and several values of h.

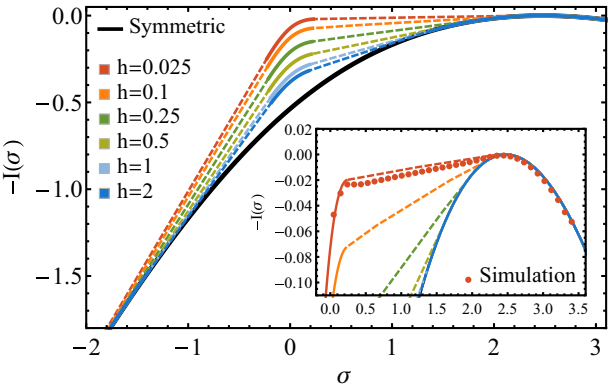

FIG. 4. (Color online) Large deviation function $I(\sigma)$ for the entropy production rate of the network in Fig. 1(b) with $x = 20$, $y = 1$, $b = 0.1$, and several different values of h. The rate function envelope was determined by the LF transform of $\psi_\omega(\lambda)$, whose two singularities require the construction of tie lines (dashed curve). Kinetic Monte Carlo simulation results (10^7 trajectories with $h = 0.025, N = 400$, and $\tau = 250$) are shown as red circles in the inset.

convex envelope of $I(\sigma)$, but in the limit of large τ, $I(\sigma)$ must converge to that envelope [22]. Further, as illustrated in Fig. 3, $\psi_\omega(\lambda)$ converges to the value of its translationally symmetric variant as $N \to \infty$ for $\lambda < \lambda^*$. Hence, we expect the large deviation rate function to equal that of the translationally symmetric network for $\sigma > \sigma_h^*$, which is illustrated in Fig. 4. In particular, the inset shows that results from kinetic Monte Carlo simulations are consistent with the convex envelope.

These observations can be further clarified and made more rigorous by an analytical treatment of the ring and triangle networks. We first focus on the ring networks. The simplicity of these networks allows us to transparently trace the origin of the cusp and the physical nature of the second dynamical phase back to the broken translational symmetry. Without loss of generality we take $x > 1$ and $\lambda < 0.5$. In the translationally symmetric variant of the ring network, the matrix $\mathbb{W}_\omega(\lambda)$ can be diagonalized by a discrete Fourier transform to give eigenvalues of the form

$$\phi^{\mathrm{TS}}(\lambda,q) = e^{-2\pi i q/N} x^{1-\lambda} + e^{2\pi i q/N} x^{\lambda} - 1 - x, \qquad (5)$$

where $0 < q < N - 1$. The superscript TS serves to emphasize the fact that Eq. (5) applies only to the translationally symmetric network. We note that the largest eigenvalue is given when $q = 0$, such that $\psi_\omega^{\mathrm{TS}}(\lambda) = \phi^{\mathrm{TS}}(\lambda,0)$. Thus, for the translationally symmetric network, the scaled cumulant generating function is smooth and the rate function resulting from the LF transform of $\psi_\omega(\lambda)$ is a simple convex function peaked around the average entropy production rate. With no broken symmetry there is only one dynamical state.

The second phase emerges in networks with the h link. We write the right eigenvector corresponding to the largest eigenvalue of $\mathbb{W}_\omega(\lambda)$ as $(f_1, f_2, \ldots f_N)$. Because the matrix is tridiagonal, we can recast the eigenvalue problem as

$$\begin{pmatrix} f_1 \\ f_2 \end{pmatrix} = B^{N-2} A_2 A_1 \begin{pmatrix} f_1 \\ f_2 \end{pmatrix}, \qquad (6)$$

where

$$B = \begin{pmatrix} \frac{\psi_\omega(\lambda)+1+x}{x^{1-\lambda}} & -x^{2\lambda-1} \\ 1 & 0 \end{pmatrix}, \qquad (7)$$

$$A_1 = \begin{pmatrix} \frac{\psi_\omega(\lambda)+h+x}{h} & -\frac{x^\lambda}{h} \\ 1 & 0 \end{pmatrix},$$

$$A_2 = \begin{pmatrix} \frac{\psi_\omega(\lambda)+1+h}{x^{1-\lambda}} & -hx^{\lambda-1} \\ 1 & 0 \end{pmatrix}. \qquad (8)$$

The eigenvalues of $\mathbb{W}_\omega(\lambda)$, in particular the largest eigenvalue $\psi_\omega(\lambda)$, can be obtained using Eq. (6), which requires that the matrix $B^{N-2}A_2A_1$ have an eigenvalue 1. The corresponding eigenvector gives (f_1, f_2). The other elements of the maximal eigenvector can be obtained using the transfer matrices B, A_1, and A_2. Specifically, for nodes $n-1, n$, and $n+1$ not touching the h link, the matrix B maps the eigenvector magnitudes (f_n, f_{n+1}) onto (f_{n-1}, f_n). The matrices A_1 and A_2 handle similar mappings on either side of the heterogeneous link.

In the large-N limit, the system with the h link can be solved using a perturbative expansion around the solution of the translationally symmetric network. Specifically, we Taylor expand in powers of $1/N$,

$$\psi_\omega(\lambda) = \psi_\omega^{\mathrm{TS}}(\lambda) + \frac{\gamma(x^\lambda - x^{1-\lambda})}{N} + O\left(\frac{1}{N^2}\right), \qquad (9)$$

where we have chosen to express the first-order coefficient in this particular form to simplify subsequent algebra. Writing

$\psi_\omega(\lambda)$ in the form of Eq. (9) allows us to express B as

$$B = B\left[\psi_\omega^{\mathrm{TS}}(\lambda)\right] + \begin{pmatrix} \frac{\gamma(x^\lambda - x^{1-\lambda})}{N x^{1-\lambda}} & 0 \\ 0 & 0 \end{pmatrix} + O\left(\frac{1}{N^2}\right). \quad (10)$$

The eigenvalues of B are handled perturbatively. To first order in $1/N$, the eigenvalues of B can be expressed as

$$k_1 = 1 - \frac{\gamma}{N} + O\left(\frac{1}{N^2}\right) = e^{-\gamma/N} + O\left(\frac{1}{N^2}\right),$$

$$k_2 = x^{2\lambda-1} + \frac{x^{2\lambda-1}\gamma}{N} + O\left(\frac{1}{N^2}\right) = x^{2\lambda-1}e^{\gamma/N} + O\left(\frac{1}{N^2}\right). \quad (11)$$

For $x > 1$ and $\lambda < 1/2$ and provided γ is finite, $k_1 > 1$ and $k_2 < 1$. Hence, when B is raised to a very large power, only the larger eigenvalue k_1 survives,

$$\lim_{N\to\infty} B^{N-2} = \lim_{N\to\infty} \frac{e^{-\gamma} + O(1/N)}{1 - x^{2\lambda-1}} \begin{pmatrix} 1 & -x^{2\lambda-1} \\ 1 & -x^{2\lambda-1} \end{pmatrix} = \frac{e^{-\gamma}}{1 - x^{2\lambda-1}} \begin{pmatrix} 1 & -x^{2\lambda-1} \\ 1 & -x^{2\lambda-1} \end{pmatrix}. \quad (12)$$

To obtain the value of the cumulant generating function we use the condition that $B^{N-2}A_2A_1$ has an eigenvalue equal to 1. From Eq. (12),

$$\lim_{N\to\infty} B^{N-2}A_2A_1 = \frac{e^{-\gamma}}{1 - x^{2\lambda-1}} \begin{pmatrix} 1 & -x^{2\lambda-1} \\ 1 & -x^{2\lambda-1} \end{pmatrix} \begin{pmatrix} \frac{x^{1-\lambda}+x^\lambda+h-x}{x^{1-\lambda}} & -hx^{\lambda-1} \\ 1 & 0 \end{pmatrix} \begin{pmatrix} \frac{x^{1-\lambda}+x^\lambda+h-1}{h} & -\frac{x^\lambda}{h} \\ 1 & 0 \end{pmatrix}$$

$$= \frac{e^{-\gamma}}{1 - x^{1-2\lambda}} \begin{pmatrix} \frac{h^2+[x^{1-\lambda}+(h-1)+x^\lambda](x-x^{1-\lambda}-h)}{hx^\lambda} & \frac{h+x^{1-\lambda}-x}{h} \\ \frac{h^2+[x^{1-\lambda}+(h-1)+x^\lambda](x-x^{1-\lambda}-h)}{hx^\lambda} & \frac{h+x^{1-\lambda}-x}{h} \end{pmatrix}. \quad (13)$$

Equation (13) allows us to solve for γ, which works out to

$$\gamma = \ln\left(\frac{x^{2(1-\lambda)} - x^{1-\lambda}(1-2h+x) - h + x - hx}{h(x^{1-\lambda} - x^\lambda)}\right). \quad (14)$$

Equations (9) and (14) provide a perturbative solution to the heterogeneous system. However, the value of γ diverges as λ approaches λ^*, where λ^* is given by

$$\lambda^* = 1 - \frac{\ln\left(\frac{1+x-2h+\sqrt{(x-1)^2+4h^2}}{2}\right)}{\ln x}. \quad (15)$$

For $\lambda \geqslant \lambda^*$, the perturbative approach is not valid. Thus, in the large-N limit, the heterogeneous network behaves exactly like the translationally symmetric network up to that value λ^*, at which point it deviates markedly. The value λ^* marks the location of the singularity in $\psi_\omega(\lambda)$ (see Fig. 5), which is also the slope of the tie line in the rate function.

The transition is accompanied by a crossover in the behavior of the eigenvectors. In particular, when the heterogenous network behaves like the translationally symmetric network, the largest eigenvector of $\mathbb{W}_\omega(\lambda)$ has an unbound or delocalized nature. In contrast, for $\lambda > \lambda^*$ the maximal eigenvector exhibits exponential localization around the heterogeneity, in agreement with kinetic Monte Carlo simulations. The study of the triangle network, while mathematically more complicated, retains the same phenomenology of a dynamic phase transition between delocalized and localized phases (see Fig. 5) and the critical value of λ^* can be determined similarly. Given the robustness to decorations of the ring, we expect similar localization transitions in more general pseudo-one-dimensional cyclical networks in the limit of a large number of states. An analytic proof of these assertions is beyond the scope of this paper. We note that the transfer matrix analysis is also amenable to a study of random disorder, where tuning of the disorder is known to induce a localization transition [23].

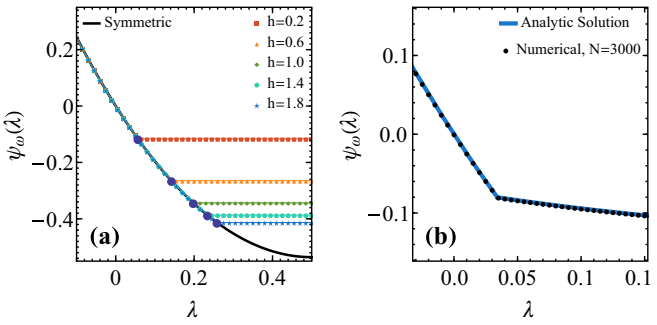

FIG. 5. (Color online) (a) Scaled cumulant generating function for the ring network with varying h. The values of λ^* predicted by our theory are plotted as large blue points in plot, which coincide with the large-N limit of the numerical calculations. (b) Singularity in the scaled cumulant generating function for the triangle network with rate constants $x = 20$, $y = 1$, $b = 0.1$, and $h = 0.1$.

In conclusion, we have demonstrated that singularities in trajectory space can in fact arise even in very simple driven cyclical kinetic networks. Previous demonstrations of such singularities have invariably involved many particle systems that are not particularly amenable to exact analytical treatment. Dynamic phase transitions in these simple driven kinetic network systems can hence serve as toy models to elucidate the various features associated with phase transitions in trajectory space. Finally, we note that cyclical or periodic driven kinetic networks find uses in many biophysical contexts. Dynamic phase transitions in such Markov state models and possible biophysical implications of the consequent large deviation statistics are subjects for future work.

We acknowledge useful discussions with Christopher Jarzynski and Frédéric van Wijland. This work was supported in part by the Director, Office of Science, Office of Basic Energy Sciences, Materials Sciences, and Engineering Division, of the U.S. Department of Energy under Contract No. DE AC02-05CH11231 (S.V. and P.L.G.). T.R.G. acknowledges

support from the NSF Graduate Research Fellowship and the Fannie and John Hertz Foundation. This research used the resources of the National Energy Research Scientific Computing Center, which was supported by the Office of Science of the U.S. Department of Energy under Contract No. DE-AC02- 05CH11231.

[1] G. E. Crooks, Phys. Rev. E **61**, 2361 (2000).
[2] C. Jarzynski, Phys. Rev. E **56**, 5018 (1997).
[3] C. Jarzynski, Annu. Rev. Condens. Matter Phys. **2**, 329 (2011).
[4] T. Bodineau and B. Derrida, Phys. Rev. Lett. **92**, 180601 (2004).
[5] T. Bodineau and B. Derrida, Phys. Rev. E **72**, 066110 (2005).
[6] C. P. Espigares, P. L. Garrido, and P. I. Hurtado, Phys. Rev. E **87**, 032115 (2013).
[7] R. J. Harris, A. Rákos, and G. M. Schütz, J. Stat. Mech. (2005) P08003.
[8] P. I. Hurtado and P. L. Garrido, Phys. Rev. Lett. **107**, 180601 (2011).
[9] J. P. Garrahan, R. L. Jack, V. Lecomte, E. Pitard, K. van Duijvendijk, and F. van Wijland, Phys. Rev. Lett. **98**, 195702 (2007).
[10] T. Speck, A. Engel, and U. Seifert, J. Stat. Mech. (2012) P12001.
[11] G. Bunin and Y. Kafri, J. Phys. A: Math. Gen. **46**, 095002 (2013).
[12] A. B. Kolomeisky and M. E. Fisher, Annu. Rev. Phys. Chem. **58**, 675 (2007).
[13] M. E. Fisher and A. B. Kolomeisky, Proc. Natl. Acad. Sci. U.S.A. **96**, 6597 (1999).
[14] Y. Tu, Proc. Natl. Acad. Sci. U.S.A. **105**, 11737 (2008).
[15] J. J. Hopfield, Proc. Natl. Acad. Sci. U.S.A. **71**, 4135 (1974).
[16] A. Murugan, D. A. Huse, and S. Leibler, Proc. Natl. Acad. Sci. U.S.A. **109**, 12034 (2012).
[17] C. H. Bennett, BioSystems **11**, 85 (1979).
[18] U. Seifert, Rep. Prog. Phys. **75**, 126001 (2012).
[19] D. T. Gillespie, J. Comput. Phys. **22**, 403 (1976).
[20] H. Touchette, Phys. Rep. **478**, 1 (2009).
[21] J. Lebowitz and H. Spohn, J. Stat. Phys. **95**, 333 (1999).
[22] H. Touchette and R. J. Harris, in *Nonequilibrium Statistical Physics of Small Systems: Fluctuation Relations and Beyond*, edited by R. Klages, W. Just, and C. Jarzynski (Wiley-VCH, Weinheim, 2013), p. 335.
[23] B. Derrida, K. Mecheri, and J. L. Pichard, J. Phys. France **48**, 733 (1987).